REPORT DOCUMENTATION PAGE

Form Approved
OMB No. 0704-0188

1. AGENCY USE ONLY (Leave blank)	2. REPORT DATE	3. REPORT TYPE AND DATES COVERED
	30 January 1996	Reprint

4. TITLE AND SUBTITLE
Numerical Simulations of Ion Beam Emissions From Negatively Charged Spacecraft

5. FUNDING NUMBERS
PR 5797
TA AF
WU 02

6. AUTHOR(S)
Joseph Wang *
Shu T. Lai

7. PERFORMING ORGANIZATION NAME(S) AND ADDRESS(ES)
Phillips Laboratory/WSSI
29 Randolph Road
Hanscom AFB, MA 01731-3010

8. PERFORMING ORGANIZATION REPORT NUMBER
PL-TR-96-2034

9. SPONSORING/MONITORING AGENCY NAME(S) AND ADDRESS(ES)

11. SUPPLEMENTARY NOTES * Jet Propulsion Lab, California Inst of Technology, Pasadena, CA
Reprinted from 34th Aerospace Sciences Meeting & Exhibit, 15-18 Jan 1996, Reno, NV

12a. DISTRIBUTION/AVAILABILITY STATEMENT
Approved for public release; distribution unlimited

12b. DISTRIBUTION CODE

13. ABSTRACT (Maximum 200 words)

Spacecraft tend to charge negatively in space plasmas at night. Positive ions ejected from a negatively charged spacecraft can escape provided that the ions are sufficiently energetic. Most ion beams devices to date generate high energy beam ions mixed with a low energy neutral gas. Charge exchange between the ions and the neutrals generate low energy ions which are attracted back to the spacecraft. In this presentation, ion beam emission effects on a negatively and differentially charged spacecraft are studied by means of numerical simulations. Electrostatic particle-in-cell with Monte Carlo collision simulation codes are developed for studying the time development of the effects of the charge exchange. Not only the low energy ions return to the spacecraft but they tend to return to the "hot" spots. The return of ions reduces the level of differential charging gradually. If the returning ions can generate secondary electrons, the level of negative spacecraft charging is also reduced.

14. SUBJECT TERMS		15. NUMBER OF PAGES
Space plasma	Ion beam	12
Spacecraft	Simulations	16. PRICE CODE
Spacecraft charging	SCATHA	

17. SECURITY CLASSIFICATION OF REPORT	18. SECURITY CLASSIFICATION OF THIS PAGE	19. SECURITY CLASSIFICATION OF ABSTRACT	20. LIMITATION OF ABSTRACT
Unclassified	Unclassified	Unclassified	SAR

PL-TR-96-2034

AIAA 96-0147

Numerical Simulations of Ion Beam Emissions from Negatively Charged Spacecraft

Joseph Wang
Jet Propulsion Laboratory
California Institute of Technology
Pasadena, CA 91109

Shu T. Lai
Phillips Laboratory
Hanscom AFB, MA 01731

34th Aerospace Sciences Meeting & Exhibit
January 15-18, 1996 / Reno, NV

Numerical Simulations of Ion Beam Emissions from Negatively Charged Spacecraft

Joseph Wang

Jet Propulsion Laboratory

California Institute of Technology, Pasadena, CA 91109

Shu T. Lai

Phillips Laboratory, Hanscom AFB, MA 01731

1. Introduction

Many space experiments and applications involve plasma beam emissions. Electron beam experiments and plasma contactor experiments have been used in several ionospheric active experiments to study beam-plasma interactions, neutralization processes, and spacecraft charging[1, 14, 9]. Ion beam experiments have been conducted on SCATHA to study spacecraft charging and discharging in geosynchronous orbit[3, 4]. Electric propulsion devices, such as ion thrusters, are currently planned to use for both commercial satellites and interplanetary space explorations.

The purpose of this paper is to study spacecraft interactions induced by positive ion beam emissions. Most ion beam devices to-date are similar to ion thrusters. An ion thruster is shown schematically in Figure 1. A neutral gas, typically xenon, is injected into an ionization chamber, in which the gas is partially ionized. The ions are accelerated electrostatically by a biased grid to form a high velocity beam, typically in the keV energy range. Electrons are emitted from a neutralizer to neutralize the ion beam. Since the ionization percentage is typically about 1 to 6% only, a significant amount of unionized neutral gas will also escape through the ion optics and from the neutralizer. Charge-exchange collisions will occur between the fast beam ions and slow neutrals.

Ion beam-spacecraft interactions may be characterized by the following parameters, n_{b0}/n_∞, E_{b0}/T_e, $E_{b0}/|e\Phi_w|$, and d_{sh}/R_{sc}, where n_{b0} and E_{b0} are the beam ion density and energy (in unit of eV) at beam exit respectively, n_∞ is the ambient plasma density, T_e the ambient plasma temperature (in unit of eV), Φ_w the spacecraft potential, d_{sh} the characteristic sheath thickness surrounding the spacecraft, and R_{sc} the characteristic dimension of the spacecraft.

Previous studies on ion beam-spacecraft interactions were mostly performed for ion thrusters [5, 6, 10, 11, 12, 18, 20]. During ion thruster operations, spacecraft potential is typically kept low by electron emission and the beam ion energy is much larger than the spacecraft potential, $E_{b0}/e\Phi_w >> 1$. Hence, the primary beam ions do not return to the spacecraft. The major interaction issue comes from the charge-exchange ions. The charge-exchange ions can leave the primary plume and backflow toward the spacecraft. In addition to contaminations, the charge-exchange ions also represents additional charging mechanisms, which may induce plasma interactions with solar arrays. Ion thruster experiments have been performed mostly either in a laboratory experiments or in the low earth orbit environment, where the ambient plasma density is relatively high. Other than the thruster exit area, the spacecraft is typically covered only by a thin sheath due to its low potential, $d_{sh}/R_{sc} << 1$. Hence, our current understanding of ion beam-spacecraft interactions mostly come from an interaction regime that can be characterized by *low-charging* and *thin-sheath* ($E_{b0}/|e\Phi_w| << 1$, $d_{sh}/R_{sc} < 1$). Under the low-charging and thin-sheath condition, although the ion beam induced spacecraft interaction is complex in nature, its effects are expected to be minimum from the spacecraft charging point of view.

In this paper, we study a different interaction regime. We consider the situation that the spacecraft is very negatively charged, the charging potential is compa-

rable or greater than the initial ion beam energy ($E_{b0}/|e\Phi_w| \sim 1$ or $E_{b0}/|e\Phi_w| > 1$), and the ambient plasma density is low so that the spacecraft is coverd by a thick sheath, $d_{sh}/R_{sc} > 1$. We shall call this interaction regime the *high-charging thick-sheath* regime ($E_{b0}/|e\Phi_w| > 1, d_{sh}/R_{sc} > 1$). Under the high-charging thick-sheath condition, significant interactions will occur between spacecraft and both the beam and charge-exchange ions within spacecraft's sheath. Hence, the interaction will greatly affect the charging and discharge of a spacecraft.

The high-charging condition can occur to spacecraft near geosynchronous altitudes, where spacecraft can be charged negatively to the kV range in the night side or during geomagnetic storms[7, 8]. A very negative charging potential can also occur when the ion beam source is operated with the neutralizer off. An example for this is the ion beam experiment on the SCATHA satellite[13]. The thick-sheath condition occurs to spacecraft in the geosynchronous orbit plasma environment or interplanetary plasma environment, where a spacecraft is always covered by a thick sheath due to the low ambient density.

This study is based on fully 3-dimensional (3-D) computer particle simulations. Recently, Samanta Roy et al. used electrostatic Particle-in-Cell (PIC) simulations to model the far-downstream region of an ion thruster and study charge exchange ion backflow[17, 18]. Wang et al. developed full particle Particle-in-Cell with Monte Carlo collision (PIC-MCC) models for single thruster as well as multiple thruster plasma plumes under both ground test and in-space conditions[20, 21]. The emphasis of these studies was to characterize the plasma plume and the charge exchange ions in the down stream region. Here, we move towards a more detailed model of spacecraft interactions induced by ion beam emission by considering ion beam emissions from a 3-dimensional, finite size, negatively charged spacecraft emersed in space plasmas. The emphasis is to study *high-charging thick-sheath* interactions induced by ion emission without neutralizing electrons. We discuss the plasma environment surrounding the entire spacecraft and the backflow of beam and charging-exchang ions under various spacecraft charging conditions.

2. Formulation and Approach

Our simulation setup is shown in Fig.2. The spacecraft is modeled as a 3-dimensional box structure with a conducting surface and a surface potential Φ_w relative to the ambient. We assume that the ambient plasma is a H^+ plasma represented by a single Maxwellian distribution. (n_∞, T_i, and T_e denote the ambient plasma density, ion, and electron temperature respectively.) The ion beam source is taken to be a 30cm Xenon ion thruster. (n_{b0} and v_{b0} denote the average beam ion density and beam velocity at thruster exit respectively.)

For convenience of the analysis, we normalize the spatial dimension by the Debye length at thruster exit $\lambda_{D0} = \sqrt{KT_e/4\pi n_{b0}e^2}$, time by the xenon ion plasma frequency at thruster exit $\omega_{pi0} = \sqrt{4\pi n_{b0}/m_{xenon}}$, ion velocity by the xenon ion acoustic velocity within the ion beam $C_s = \sqrt{T_e/m_{xenon}}$, and the potential by the ambient electron temperature T_e.

The equilibrium charging state for a uniformly conducting body is determined by the total current balance condition: $\Sigma I(\Phi_w) = 0$. For our problem, the charging equation is written as

$$\Sigma I(\Phi_w) = I_i - I_e - I_{bi} + I_{be} + I_{return} = 0 \qquad (1)$$

where I_i and I_e are ion and electron current from the ambient plasma respectively, I_{bi} is the beam ion current, and I_{be} is the electron current emitted from the neutralizer. I_{return} is the beam induced return current, which includes both the beam ion current I_{bir} and the charge exchange ion current I_{cexr} collected by the spacecraft.

From the probe theory, the ambient electron and ion current to a negatively charged, stationary conducting sphere under the thick-sheath condition is given by[15]:

$$I_e = J_{e\infty}\exp(\Phi_w/T_e)A_{sc} = en_\infty\sqrt{\frac{T_e}{2\pi m_e}}\exp(\Phi_w/T_e)A_{sc} \qquad (2)$$

$$I_i = J_{i\infty}(1-\Phi_w/T_i)A_{sc} = en_\infty\sqrt{\frac{T_i}{2\pi m_e}}(1-\Phi_w/T_i)A_{sc} \qquad (3)$$

where A_{sc} is the spacecraft area. However, to calculate I_{return}, one needs to obtain the self-consistent solution of space charge distribution, electric field, and particle orbits.

We have developed a set of full particle and hybrid PIC-MCC simulation codes to simulate ion thruster plasma interactions[20]. The numerical models and algorithms have been discussed in detail in Ref[20, 22, 23]. Since the focus of this paper is on ion interactions with a negatively charged body, simulation results presented in this paper are derived from a hybrid PIC-MCC code. The electron density is assumed to follow the Boltzmann distribution $n_e = n_{ref}\exp((\Phi-\Phi_{ref})/T_e)$, where n_{ref} and Φ_{ref} are the electron density and potential at a reference point respectively. In particular, the ambient electron density surrounding a negatively charged spacecraft is given by

$$n_e = n_\infty\exp(e\Phi/KT_e) \qquad (4)$$

The ambient ion density, which is much lower than the beam ion density, is assumed to be a constant background. The beam ions and charge-exchange ions are treated as test particles.

At each time step, the beam ions are injected into the simulation domain from the beam source exit. Experiments have shown that the beam ions are emitted with a spatial density distribution close to that of a Gaussian distribution and a divergence angle of about 15^o to 20^o. To simulate the ion beam current emitted from a thruster, the particles are injected in such a way that the resulting flux has a density in Gaussian distribution at the exit plane

$$|J_{bi}| = J_{bmax} \exp(-(r/r_T)^2), \quad r \leq r_T \tag{5}$$

where J_{bmax} is the density at the thruster exit center, r is the distance to the center on the thruster exit plane, and r_T is the thruster radius. In this study, we take the divergence angle to be 15^o.

In an ion thruster, not all the propellant is ionized due to discharge chamber inefficiencies and operating constraints. Along with the beam ions, significant amount of neutrals also flow out of the thruster and form a neutral plume. In the simulation, the neutral plume is modeled as a steady background. As in [17], the density distribution of the neutral plume is modeled as that of a free molecular flow from a point source located at one thruster radius r_T behind the thruster exit[17]. Hence, the density distribution of the neutral plume is given by:

$$n_n(R,\theta) = a n_{n0}(1 - (1 + (\frac{r_T}{R})^2)^{-1/2}) \cos\theta \tag{6}$$

where n_{n0} is the average neutral density at thruster exit, R is the distance to the point source, θ is the angle between R and the downstream axis, and a is a correction factor. n_{n0} is related to the ion beam via the following relationship[17]:

$$n_{n0} \simeq \frac{4 n_{b0} v_{b0}}{C}(\frac{1}{\eta_p} - 1) \tag{7}$$

where $C = \sqrt{8kT_w/\pi m_{xenon}}$ is the mean thermal speed of the neutrals, and η_p is the propellant utilization efficiency. Typically, the thruster discharge chamber wall temperature is $T_w \simeq 500$K. For normal thruster operations, η_p range from 0.7 to 0.9. A significant higher neutral plume density may also be obtained either due to low propellant utilization or through extra neutral sources.

Charge-exchange collisions will occur between beam ions and neutrals. The charge-exchange collision cross section for xenon can be expressed by[16, 17]:

$$\sigma_{cex} = (k_1 \ln v_{bi} + k_2)^2 \times 10^{-20}\ m^2 \tag{8}$$

where v_{bi} is beam ion velocity with unit in m/s, $k_1 = -0.8821$, and $k_2 = 15.1262$.

As in a standard PIC-MCC code[2], the trajectory of each particle is integrated from

$$\frac{dm\vec{V}}{dt} = \vec{F} = q(\vec{E} + \vec{V} \times \frac{\vec{B}}{c}), \quad \frac{d\vec{x}}{dt} = \vec{V} \tag{9}$$

using a standard leapfrog scheme. The probability that a charged particle suffers a collision within time t is given by

$$P(t) = 1 - \exp(-\int_0^t \nu(t)dt) \tag{10}$$

where $\nu = n_n(\vec{x}) v \sigma(v)$ is the collision frequency, and $\sigma(v)$ is given by eq(8). Since the neutral density, which is defined on grid points, is nonuniform, the collision frequency for each particle is obtained by interpolating the neutral density $n_n(x,y,z)$ to the particle position, similar to the field interpolation in a PIC code. At each time step, for each particle, the accumulated collision probability in the time step is calculated, and a random number P_{ran} evenly distributed between 0 and 1 is then chosen to determine whether a collision has occured. The self-consistent electric field is than obtained from the Poisson's equation

$$\nabla^2 \Phi = -4\pi\rho \tag{11}$$

Finally, since we are simulating a thick sheath situation, computationally it is not feasible to set the simulation domain large enough for the outer boundary to be the undisturbed ambient. Hence, a Neumann condition $\nabla \Phi_n = 0$ is used at all outer boundaries of the simulation domain. In this paper, the number of grid points used for the simulation domain is $47 \times 47 \times 47$ and the number of test particles is in the range of 10^6.

3. Results and Discussions

In this section, we discuss simulation results. We consider the spacecraft configuration shown in Figure 2a (no solar array). The spacecraft is taken to be a cubic box with dimension $1m \times 1m \times 1m$. The ion beam source is taken to be a 30cm Xenon ion thruster. The beam ions exit the thruster with an energy of $E_{b0} = 800$eV Since our main purpose here is to study ion beam interactions, the ion beam current is taken to be much less than the value used for propulsion applications. To cover a range of interaction parameters, n_{b0}/n_∞,

E_{b0}/T_e, $E_{b0}/|e\Phi_w|$, and d_{sh}/R_{sc}, we present four simulation cases, as summarizd in Table 1.

In simulation cases A and B, we take the ambient plasma environment to be a "cold" plasma with $n_\infty \simeq 10^2\ cm^{-3}$, $T_i = 0.5T_e$ and $T_e \simeq 8$eV ($E_{b0}/T_e \simeq 100$). (Ambient current densities: $J_{i\infty} \simeq 1.3\times10^{-7}\ A/m^2$ and $J_{e\infty} \simeq 7.5\times10^{-6}\ A/m^2$.) We take the average beam ion density at thruster exit to be $n_{b0} \simeq 10^3 n_\infty \simeq 10^5\ cm^{-3}$. (Average beam current density at exit $J_{b0} = |e|n_{b0}v_{b0} \simeq 5.3\times10^{-4}\ A/m^2$.) In case A, we assume the ion beam source is operated with the neutralizer on, and hence, the beam is quasineutral. Since there is no charging mechanism involved in this situation, the spacecraft can be charged only to a low potential. We take the spacecraft potential to be $-\Phi_w/T_e \simeq 3$ ($E_{b0}/|e\Phi_w| \simeq 33.3$). Hence, case A is a low-charging case.

In case B, we assume that the ion beam source is operated with the neutralizer off. Hence, the ion beam is only neutralized by the ambient electrons. (The ambient electron density is given by eq(4).) It's interesting to estimate the maximum charging potential a spacecraft can reach under this condition. From eq(1), the maximum charging potential is given by $I_i - I_{bi} \simeq 0$, assuming there are no returning ion current and electron current. Hence, we have

$$-\frac{\Phi_w}{T_e} \leq \frac{1}{2\pi}\frac{n_{b0}}{n_\infty}\frac{A_T}{A_{sc}}\sqrt{\frac{m_p}{m_{xenon}}}\sqrt{\frac{T_i}{T_e}}\sqrt{\frac{2E_{b0}}{T_e}} - 1$$

where A_T is the ion beam emitting area. For the parameters used here, we found $\Phi_w/T_e \sim -47$. We shall use this value for Φ_w in case B ($E_{b0}/|e\Phi_w| \simeq 2.1$).

In simulation cases C and D, we take the ambient plasma environment to be a "warm" plasma with $n_\infty \simeq 10^2\ cm^{-3}$, $T_i = 0.5T_e$ and $T_e \simeq 80$eV ($E_{b0}/T_e \simeq 10$). (Ambient current densities: $J_{i\infty} =\simeq 4.1\times10^{-7}\ A/m^2$ and $J_{e\infty} \simeq 2.4\times10^{-5}\ A/m^2$.) We take the average beam ion density at thruster exit to be $n_{b0} \simeq 10^4 n_\infty \simeq 10^6\ cm^{-3}$. (Average beam current density at exit $J_{b0} \simeq 5.3\times10^{-3}\ A/m^2$.) Again, we assume that the ion beam source is operated with the neutralizer off, and the spacecraft is charged to some very negative potential. In the high-charging case, it is not possible to estimate the charging potential *a prio* because the return current can no longer be neglected. In case C, we take $-\Phi_w/T_e \simeq 10$, i.e. $E_{b0}/|e\Phi_w| \simeq 1$. In case D, we take $-\Phi_w/T_e \simeq 75$, i.e. $E_{b0}/|e\Phi_w| \simeq 0.13$.

Since the ambient Debye length is larger than the spacecraft dimension, the spacecraft is covered by a thick sheath in all simulation cases here. In the simulation results presented here (with the exception of Figure 3), the spacecraft is located at $2 \leq x \leq 16$, $15 \leq y \leq 29$, and $15 \leq z \leq 29$. The thruster exit center is located at $x = 18$, $y = 22$, and $z = 22$. The grid resolution is given by the Debye length at thruster exit $\lambda_{D0} \simeq 6.7$cm.

Cases	$E_{b0}/\lvert e\Phi_w\rvert$	n_{b0}/n_∞	E_{b0}/T_e	$-\Phi_w/T_e$
A	33.3	10^3	100	3
B	2.1	10^3	100	47
C	1.0	10^4	10	10
D	0.13	10^4	10	75

Table 1: Simulation cases

The simulation results are shown from Figure 3 through Figure 12. In the following, most contour plots are for a xy plane cutting through the spacecraft and thruster center at $z = z_{thruster} = 22$. Hereafter, this plane will be referred to as the "center xy plane". All particle plots are for particles located within a layer of ±1 cell of the center xy plane. Hereafter, this layer will be referred to as the "center layer".

Figure 3 shows the potential contours on the center xy plane for the no beam situation. Figure 4 shows the neutral plume density contours on the center xy plane. Since the neutral density decreases as R^{-2}, most of the charge-exchange ions are generated close to the thruster exit.

The results from simulation case A are shown in Figure 5 (Φ contours and $\vec{E}$ field vectors on the center xy plane) and Figure 6 (beam ions and charge-exchange ions within the center layer). This case is similar to the ion thruster situation. Since $E_{b0}/|e\Phi_w| >> 1$ and the beam is quasineutral, the beam ions are not influenced by the potential field. The structure of the potential field is dominated by the disturbance from the high density ion beam. The potential in the beam center Φ_{center} and the ambient potential Φ_∞ has the following approximate relation:

$$\Phi_{center} - \Phi_\infty \simeq T_e \ln n_{beam}/n_\infty$$

Further away from the thruster, the potential diffuse to that of the ambient. Collisions between the beam ions and the neutral background generate charge exchange ions. The charge exchange ion production rate is proportional to the neutral density shown in Figure 4. In contrast to the beam ions, the motion of the charge exchange ions are influenced by the potential field due to their low kinetic energy. The potential field influences the charge exchange ions in two ways. First, charge exchange ions produced near the thruster exit will be accelerated towards the thruster exit. This backflow

may cause potential erosion on the acceleration grids. Second, since the plume center has a higher potential, charge exchange ions produced within the beam can flow radially outward the beam region. It is well recognized that, once outside the plume, charge exchange ions may become a potential contamination source. Except for those charge-exchange ions generated right downstream of the thruster, the collection of charge-exchange ions by the spacecraft is similar to the current collection by a probe in the orbital motion limited regime. As the $\vec{E}$ vector plot in Figure 5b and charge-exchange ion plot in Figure 6b clearly indicate, a symmetrically shaped spacecraft charged to a few T_e can not collect a significant amount of charge-exchange ion current.

The results from simulation case B are shown in Figure 7 (Φ contours and $\vec{E}$ field vectors) and Figure 8 (beam ions and charge-exchange ions within the center layer). Figure 7 clearly shows that the structure of the potential field is a combined result of the surface potential and the beam space charge. The surface potential generates a sheath covering the spacecraft. On the other hand, the potential structure generated by the beam is similar to the expansion fan structure associated with a plasma expanding into a vacuum[19]. The transition of the potential structure from that dominated by the sheath to that dominated by the beam is evident in Fig. 7. Since $|e\Phi_w|$ and E_{b0} is comparable in this case ($E_{b0}/|e\Phi_w| \simeq 2.1$), the beam ions are affect by the potential field (the slowing down of beam ions are evident in Figure 8c). The $\vec{E}$ field structure shown in Figure 7b and charge exchange ion plot in Figure 8 also indicate that the charge-exchange ions not only flow radially outward the beam region but also backflow to orbit around the spacecraft. The charg-exchange ions collected by the spacecraft is $I_{cexr}/I_{i\infty} \sim 3 \times 10^{-7}$.

The results from simulation case C are shown in Figure 9 and Figure 10. Due to the high beam density, the sheath near the thruster exit is much thinner than the sheath covering the spacecraft. Since $E_{b0}/|e\Phi_w| \simeq 1$ in this case, the beam ions are stoped and pulled back over the distance of the thruster sheath. Hence, in addition to the charge-exchange ions, the spacecraft also collects the beam ions. In case D, we further increase the spacecraft potential so that $E_{b0}/|e\Phi_w| \simeq 0.13$ (Figures 11 and 12). Case D is the opposite limit of case A in that the structure of the potential field is dominated by the spacecraft sheath. The ion beam only represents a small perturbation. The entire population of the beam ions and charge-exchange ions are trapped within the potential well of the spacecraft and will be collected. Of course, this will led to the discharging of spacecraft.

4. Summary and Conclusions

We have developed a 3-D PIC-MCC simulation model to study ion beam-spacecraft interactions. Simulation results are presented for ion beam emissions under several charging conditions. The interaction characteristics are discussed for both the *high-charging* and the *low-charging* regime. When the interaction is within the low-charing regime ($E_{b0}/|e\Phi_w| >> 1$), such as that in an ion propulsion application, the interactions mainly come from the charge-exchange ions. We find that charge-exchange ions typically does *not* alter a spacecraft's charging environment. When the interaction is within the high-charing regime ($E_{b0}/|e\Phi_w| < 1$), both the charg-exchange ions and the beam ions will return to the spacecraft. The returning beam ions can led to the discharging of the spacecraft. It is also interesting to note that ion beam emissions in the high-charging regime may be used to discharge a spacecraft efficiently. For instance, a spacecraft often have "hot" spots on dielectric surfaces and it is difficult to discharge these spots by electron emission from the metallic ground. In this situation, not only the ions return to the spacecraft but they tend to land on these "hot" spots, where the potential is more negative. This reduces the level of differential charging gradually. While this study has focused on the returning current under a given spacecraft potential, in future we plan to include a dynamic calculation of the spacecraft potential and study the time development of spacecraft charging/discharge during an ion beam emission. Other interaction issues, such as plasma waves and instabilities induced by an ion beam, will also be studied.

Acknowledgement

We would like to thank D. Brinza, J. Brophy, and R. Samanta Roy for many useful discussions. This work was carried out by the Jet Propulsion Laboratory, California Institute of Technology under a contract with NASA. Access to the Cray YMP supercomputer used in this study was provided by funding from NASA Offices of Mission to Planet Earth, Aeronautics, and Space Science.

References

[1] C. Beghin, J. Lebreton, B. Maehlum, J. Troim, P. Ingsoy, and J. Michau Phenomena induced by charged particle beams, *Science*, 225, 1984, pp188–194.

[2] C.K. Birdsall, Particle-in-Cell charged particle simulations, plus Monte Carlo collisions with neutral atoms, PIC-MCC *IEEE Trans. Plasma Science*, 19(2), 1991, pp65–85.

[3] H. Cohn et al., A comparison of three techniques of discharging satellites, in Spacecraft Charging Technology, N. Stevens and C. Pike(eds), 19(2), *NASA CP-2182*, 1981

[4] H. Cohn and S.T. Lai, Discharging the p78-2 satellite using ions and electrons, *AIAA-82-0266*, 1982

[5] M.R. Carruth Eds, Experimental and analytical evaluation of ion thruster/spacecraft interactions. JPL Publication 80–92, 1981.

[6] W.D. Deininger, Electric propulsion produced environments and possible interactions with the SP-100 power system. *AIAA 85-2046*, 1985.

[7] H.B. Garrett, The charging of spacecraft surfaces, *Rev. Geophys. Space Phys.*, 19(4), 1981, pp577–616.

[8] M. Gaussenhoven and E. Mullen, Geosynchronous environment for severe spacecraft charging, *J. Spacecraft Rockets*, 20(1), 1983, pp20–34.

[9] I. Katz, J. Barfield, J. Burch, J. Marshall, W. Gibson, and T. Neubert, Interactions between the space Experiments with particle accelerators plasma contactor and the ionosphere, *J. Spacecraft Rockets*, 31(6), 1994, pp1079–1084.

[10] I. Katz, D. Parks, M. Mandell, and G. Schnuelle, Parasitic current losses due to solar-electric propulsion generated plasmas, *J. Spacecraft Rockets*, 19(2), 1982, pp129–132.

[11] Kaufman, Charge-exchange plasma generated by an ion thruster, *NASA CP-135318*, 1977.

[12] W. Kerslake and L. Ignaczak, SERT II 1980 extended flight thruster experiments, *AIAA 81-0665*, 1981.

[13] S.T. Lai, An overview of electron and ion beam effects in charging and discharging of spacecraft, *IEEE Trans. Nucl. Sci.*, 36, 1989, pp2027–2032.

[14] T. Neubert, P. Banks, B. Gilchrist, A. Fraser-Smith, and P. Willamson, The interaction of an artificial electron beam with the earth's upper atmosphere: effects on spacecraft charging and the near-plasma environment, *J. Geophys. Res.*, 95(8), 1990, pp12209–12217.

[15] S. Prokopenko and J. Laframboise, High voltage differential charging of geostationary spacecraft, *J. Geophys. Res.*, 85, 1980, pp4125.

[16] D. Rapp and W. Francis, Charge-exchange between gaseous ions and atoms, *J. Chem. Phys.*, 37, 1962, pp2631–2645.

[17] R. Samanta Roy, Numerical simulation of ion thruster plume backflow for spacecraft contamination assessment, Ph.D. thesis, MIT, 1995.

[18] R. Samanta Roy, D. Hastings, and N. Gatsonis, Modeling of ion thruster plume contamination, *AIAA 95-3138*,1994.

[19] J. Wang and D. Hastings, Ionospheric plasma flow over large high-voltage space platforms. II: The formation and structure of plasma wake, *Physics of Fluids B*, 4(6), 1992, pp1615–1629.

[20] J. Wang and J. Brophy, 3-D Monte-Carlo particle-in-cell simulations of ion thruster plasma interactions, *AIAA 95-2826*,1995.

[21] J. Wang, J. Brophy, P. Liewer, and G. Murphy, Modeling Ion Thruster Plumes, *AIAA 95-0596*,1995.

[22] J. Wang, R. Biasca, and P. Liewer, , 3D electromagnetic Monte Carlo particle-in-cell simulations of critical ionization velocity experiments in space to be published in *J. Geophys Res.*, 1995

[23] J. Wang, P. Liewer, and E. Huang, 3-D particle-in-cell with Monte Carlo collision simulations on three MIMD parallel computer, submitted to *J. Supercomputing*, 1995.

Figure Captions

Figure 1: Ion thruster (Upper). Space charge potential along the ion beam (Lower).

Figure 2: Model setup. a) spacecraft. b) spacecraft with solar arrays.

Figure 3: Potential contours on the center xy plane for no beam situation.

Figure 4: Neutral plume density contours on the center xy plane.

Figure 5: Potential contours (a) and $\vec{E}$ field (b) on the center xy plane. Simulation case A.

Figure 6: Beam ion positions (a) and charge-exchange ion positions (b) within the center layer. Simulation case A.

Figure 7: Potential contours (a) and $\vec{E}$ field (b) on the center xy plane; Potential contours on the $z = 15$ xy cutting plane (c). Simulation case B.

Figure 8: Beam ion positions (a), charge-exchange ion positions (b), and beam/charge-exchange ion v_x vs. x (c) within the center layer. Simulation case B.

Figure 9: Potential contours on the center xy plane (a) and on the $z = 15$ xy cutting plane (b). Simulation case C.

Figure 10: Beam ion positions (a), beam ion v_x vs. x (b), charge-exchange ion positions (c), and charge-exchange ion v_x vs. x (d) within the center layer. Simulation case C.

Figure 11: Potential contours on the center xy plane (a) and on the $z = 15$ xy cutting plane (b). Simulation case D.

Figure 12: Beam ion positions (a), beam ion v_x vs. x (b), charge-exchange ion positions (c), and charge-exchange ion v_x vs. x (d) within the center layer. Simulation case D.

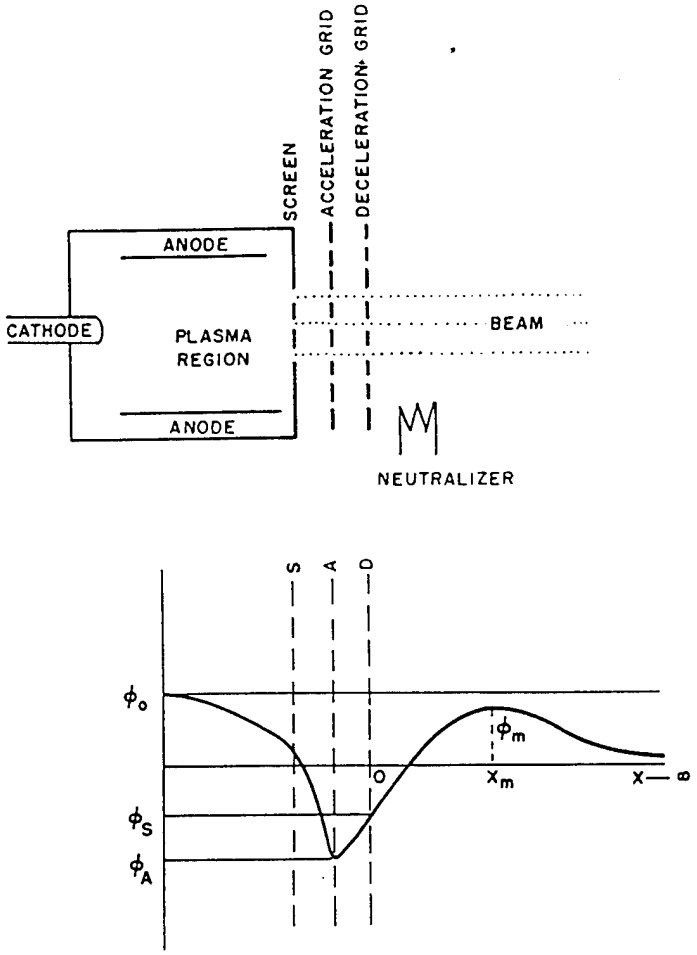

Figure 1

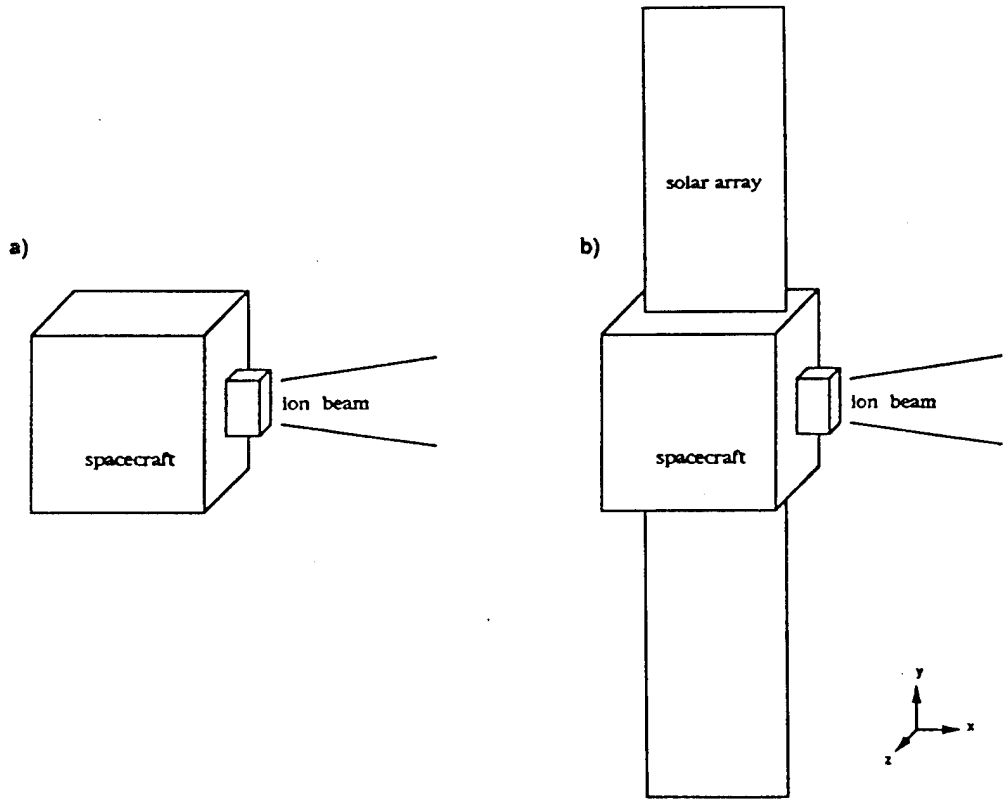

Figure 2

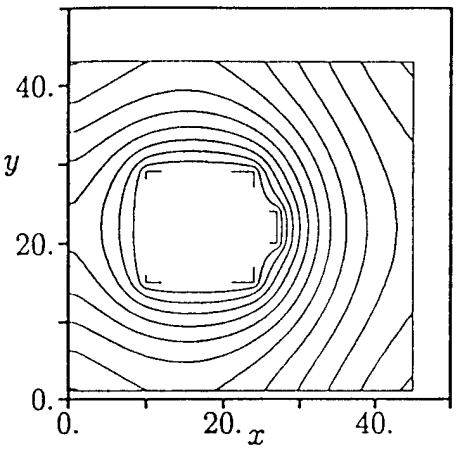

Figure 3

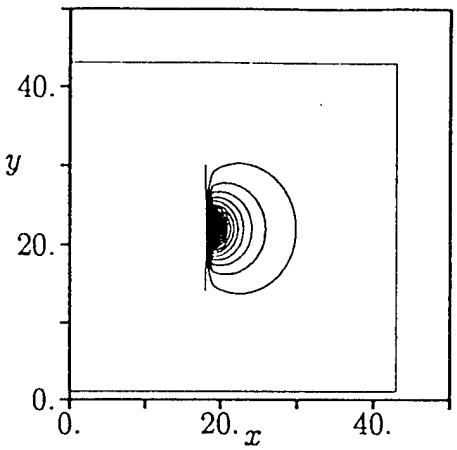

Figure 4

a) Φ Cutting plane at ZVIEW= 22.

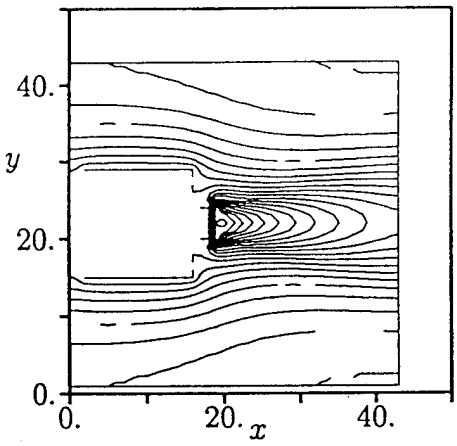

b) $\vec{E}$ Cutting plane at ZVIEW=22.

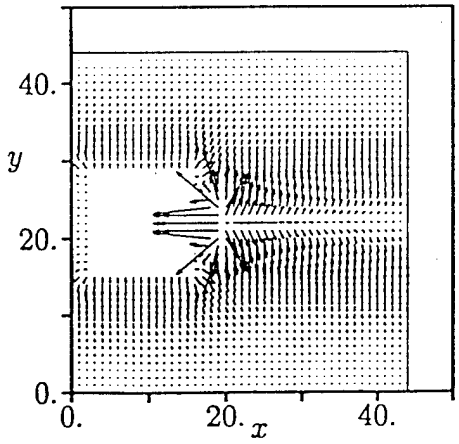

Figure 5

a) beam ion position

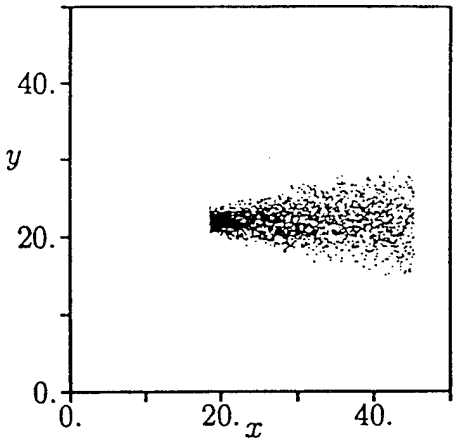

b) charge-exchange ion position

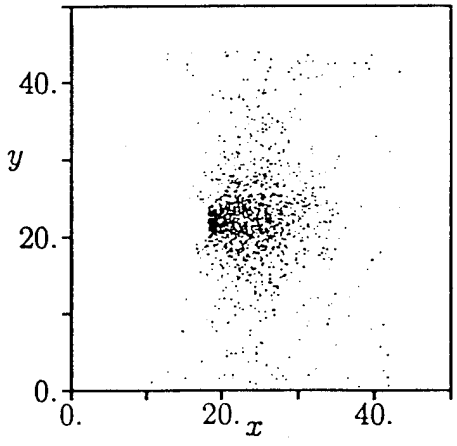

Figure 6

a) Φ Cutting plane at ZVIEW= 22.

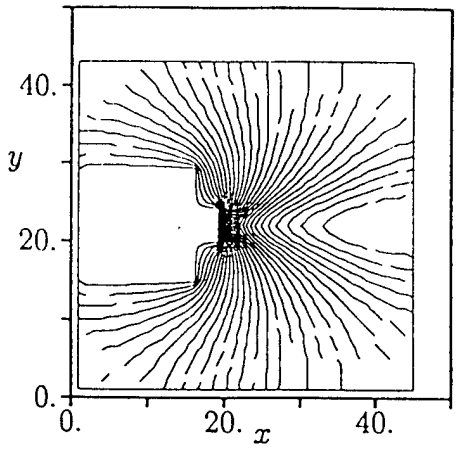

b) $\vec{E}$ Cutting plane at ZVIEW=22.

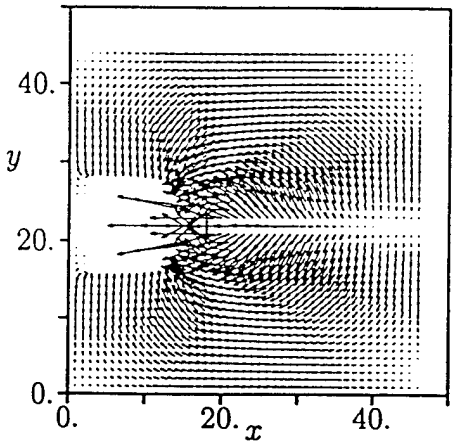

c) Φ Cutting plane at ZVIEW= 15.

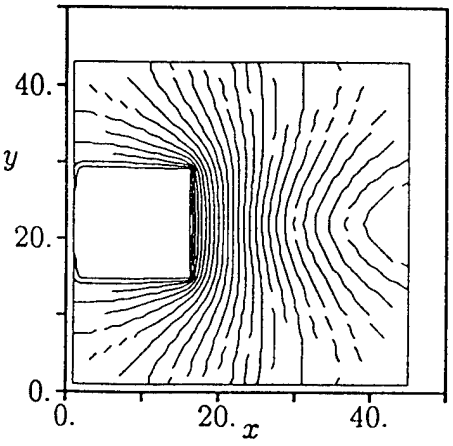

Figure 7

a) beam ion position

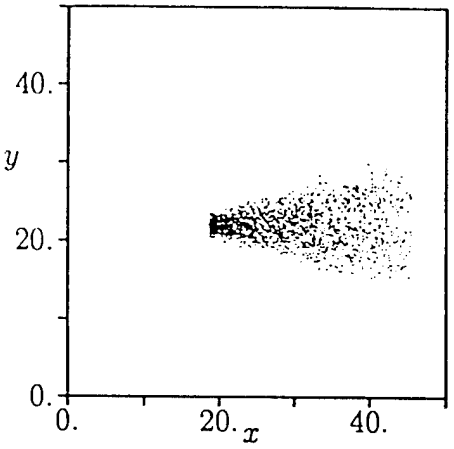

b) charge-exchange ion position

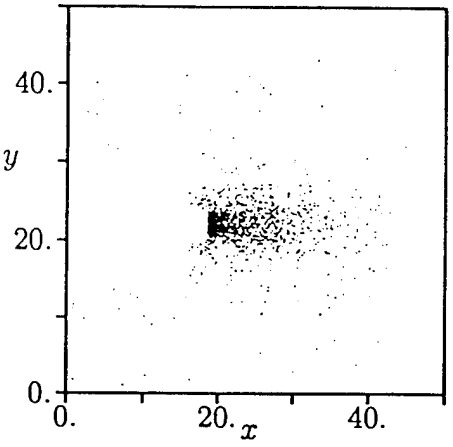

c) phase space

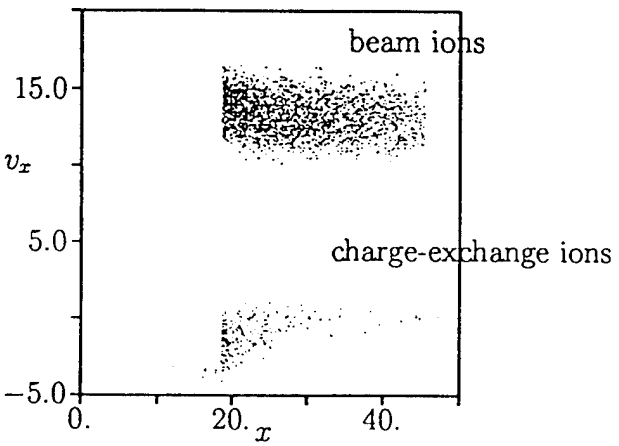

Figure 8

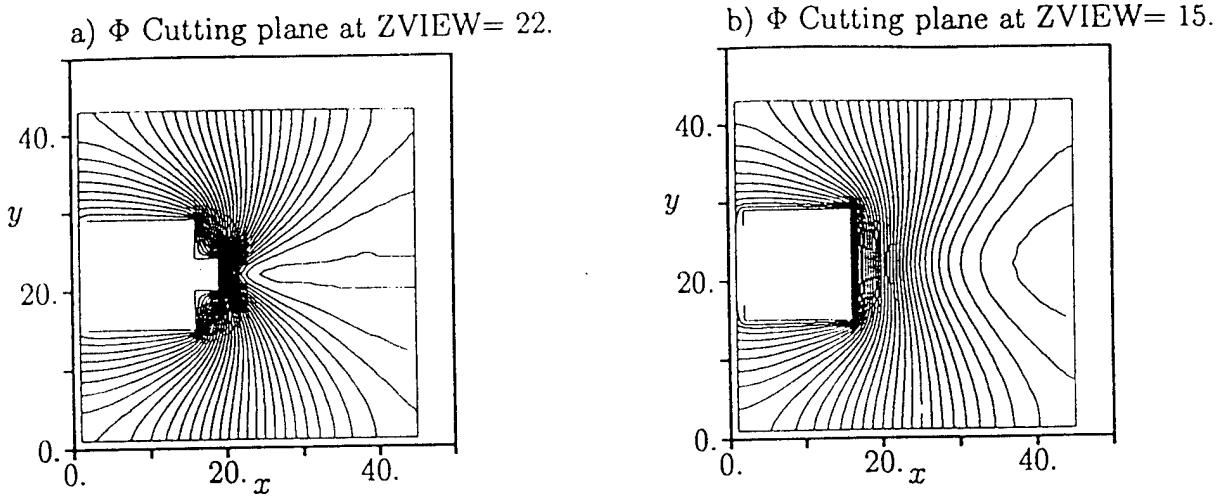

Figure 9

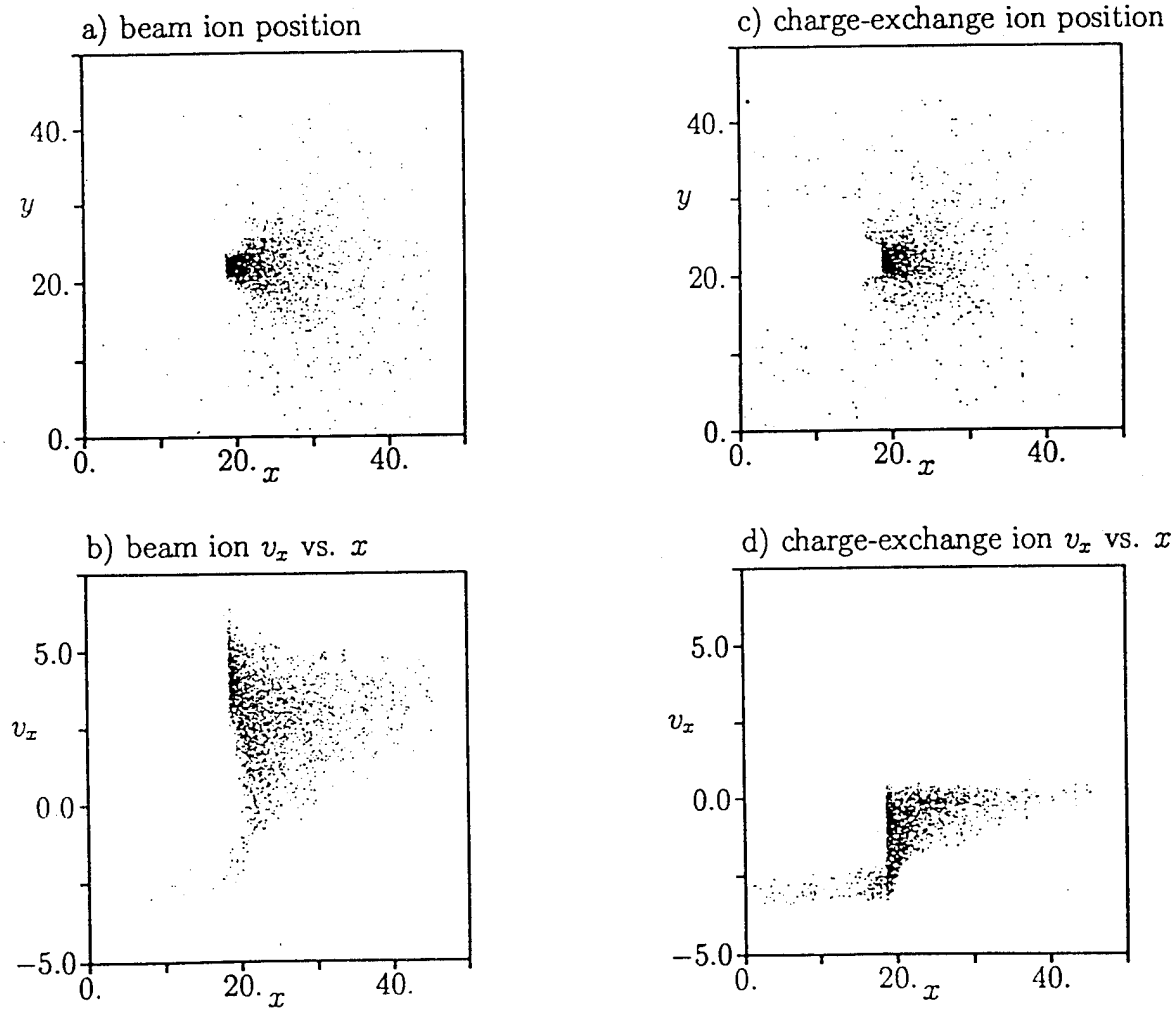

Figure 10

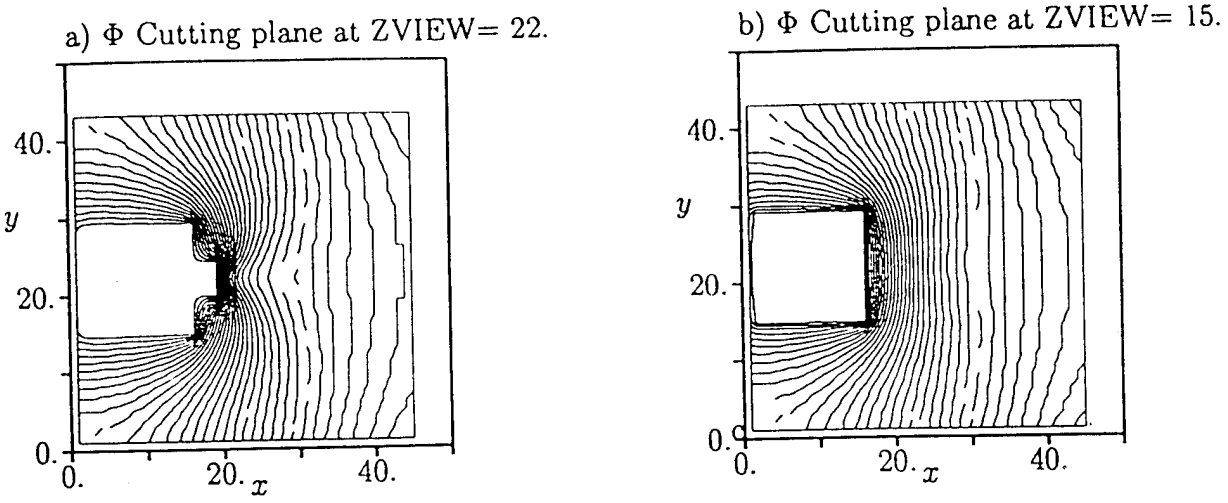

Figure 11

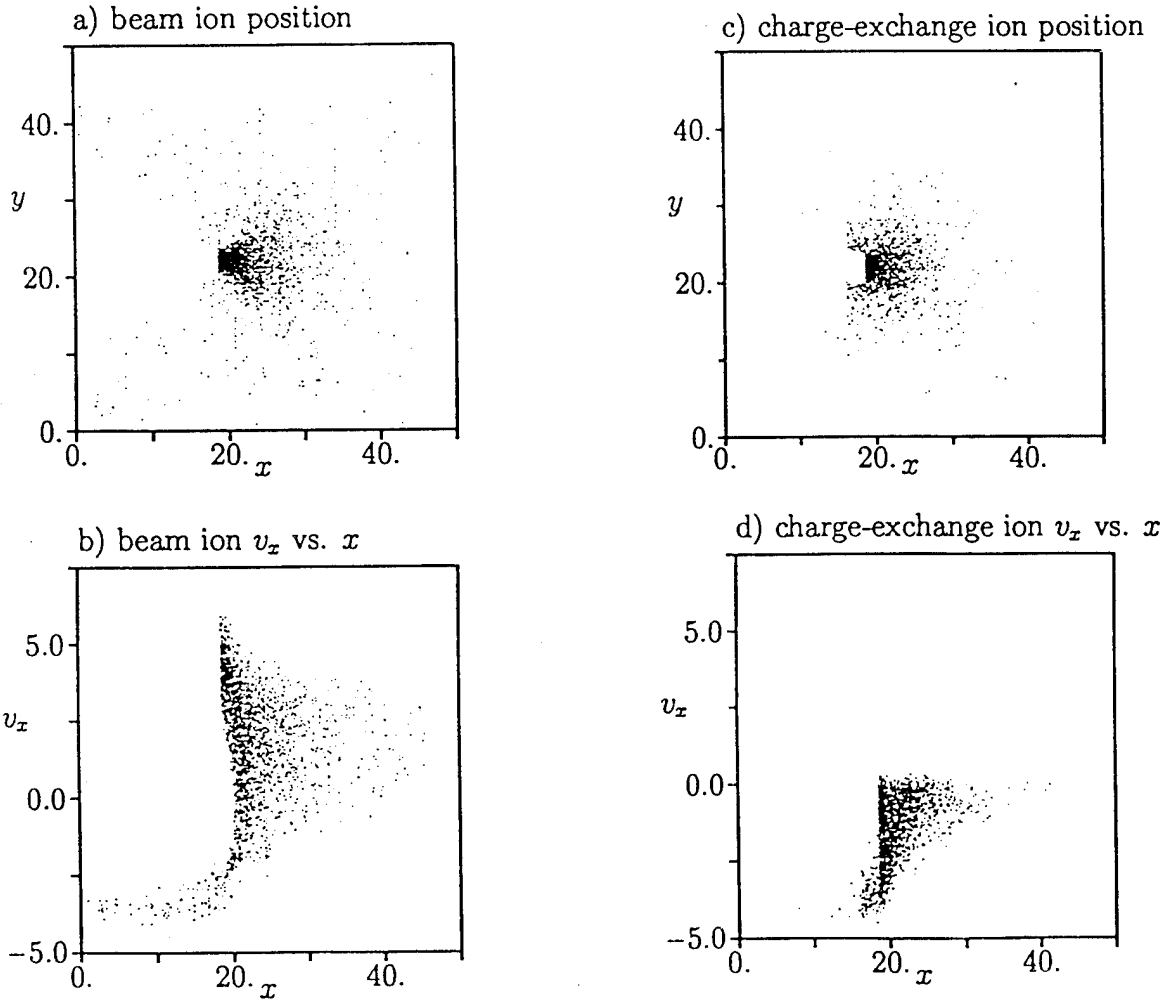

Figure 12